International Journal of Heat and Mass Transfer 107 (2017) 105–111

Contents lists available at ScienceDirect

International Journal of Heat and Mass Transfer

journal homepage: www.elsevier.com/locate/ijhmt

Enhancement of critical heat flux and superheat through controlled wettability of cuprous-oxide fractal-like nanotextured surfaces in pool boiling

Hong Seok Jo [a,1], Seongpil An [a,1], Hyun Goo Park [a], Min-Woo Kim [a], Salem S. Al-Deyab [b], Scott C. James [c], Jeehoon Choi [d,*], Sam S. Yoon [a,*]

[a] School of Mechanical Engineering, Korea University, Seoul 02841, Republic of Korea
[b] Petrochem. Research Chair, Dept. of Chem., King Saud Univ., Riyadh 11451, Saudi Arabia
[c] Dept. of Geosciences and Mech. Eng., Baylor University, Waco, TX 76798, USA
[d] LG Electronics Inc., Seoul, Republic of Korea

ARTICLE INFO

Article history:
Received 8 September 2016
Received in revised form 8 November 2016
Accepted 8 November 2016

Keywords:
Electrospinning
Electroplating
Cuprous oxide
Pool boiling
Superheat temperature
Critical heat flux

ABSTRACT

Highly nanotextured surfaces fabricated by electroplating are demonstrated in pool-boiling applications. Nickel-chrome wires were electroplated with copper and then annealed to cuprous oxide before being subject to Joule heating in a water bath. Vapor bubbles formed whose buoyant rise removed heat and promoted cooling. Hydrophobic and hydrophilic nanotextured surfaces could be tuned by varying the electroplating time. A hydrophobic surface enhanced bubble dynamics to locally decrease the surface temperature of the wire, which, in turn, enhanced superheat and the effective heat transfer coefficient. Conversely, a hydrophilic surface, characterized by a "fractal-like" surface decorated with numerous nucleation sites, increased the overall heat removal and thus the critical heat flux. These nanotextured surfaces were characterized by scanning electron microscopy and their pool boiling dynamics were visualized with a high-speed CCD camera. Theoretical heat-transfer estimates compared well with experimental data.

1. Introduction

Compact computing hardware devices have seen tremendous growth with increased market penetration of the Internet. These electronic devices have been miniaturized by nanoelectronics. However, advances in nanoelectronics are hindered by stringent thermal management requirements. For example, the normal operating regime for silicon chips typically requires a chip temperature below 70 °C. Above this, chip reliability or efficiency decreases by 10% for every 2 °C temperature rise [1]. Thermal management is also challenged by the demand for greater heat flux.

Fan-based air cooling cannot achieve the necessary cooling requirements at a sufficiently low noise level, especially given the confined space constraints of these devices [2]. The high heat transfer coefficients associated with pool boiling is an attractive solution because these systems can transfer a lot of heat at low wall superheats [3]. Pool boiling heat transfer has been proven in a wide variety of applications from nuclear power plant reactor cooling to vapor chambers, thermosyphons, and others, although improvements in critical heat flux (CHF) and heat transfer coefficient are still sought [4–6].

Heat transfer in pool boiling depends not only upon the number of nucleation sites, but also upon the corresponding rate of bubble formation, both of which are associated with surface-liquid interfacial characteristics such as surface wettability and surface roughness. Surface-liquid interfacial characteristics can be classified into two broad categories: hydrophilic and hydrophobic. Hydrophilic surfaces have a high surface density of nucleation sites, which serve to increase CHF [7–9]. On the other hand, hydrophobic surfaces (with fewer nucleation sites per unit area) release bubbles more frequently [10–13]. These frequently release bubbles increase convective cooling resulting in a decreased surface temperature and correspondingly larger superheat (ΔT) and effective heat transfer coefficient. It is important to note, however, that the enhanced superheat promoted by the frequent bubble release of a hydrophobic surface does not guarantee an increase in CHF, which is always increased by a hydrophilic surface (more

* Corresponding authors.
E-mail addresses: choijeehoon@gmail.com (J. Choi), skyoon@korea.ac.kr (S.S. Yoon).
[1] These authors have equally contributed.

http://dx.doi.org/10.1016/j.ijheatmasstransfer.2016.11.029
0017-9310/

nucleation sites and more total bubbles). These two ends of the spectrum (hydrophilic and hydrophobic surfaces) cannot exist simultaneously, but if the effects of each are understood, the surface can be properly tuned to optimize either superheat or CHF.

In this study, we electroplate a nickel-chrome (NiCr) wire with nanotextured cuprous oxide (Cu_2O) before running Joule heating experiments. The degree of nanotexturing is controlled by changing the electroplating time, forming anything from a moderately rough hydrophobic surface to a spikey, fractal-like hydrophilic surface with many nucleation sites. We develop these nanotextured surfaces and compare the effects of their morphology on superheat and CHF enhancement so that the most appropriate surface for a particular application can be selected.

2. Experimental

2.1. Materials

A NiCr wire (ThyssenKrupp VDM) with average diameter of 0.296 mm (R_0) with initial wire resistance of 15.4 ohm/m was used for pool boiling test. A copper-plating solution composed of 500 mL of distilled water, 80 g of copper sulfate (Sigma-Aldrich), 25 g of sulfuric acid (Matsunoen Chemicals), 2.5 g of hydrochloric acid (Sigma-Aldrich), and 50 g of formaldehyde (Sigma-Aldrich) was used to electrodeposit copper onto the surface of the wire. To obtain a homogeneous solution, it was magnetically stirred for 1 h at room temperature (25°C).

2.2. Cuprous oxide nanotexturing on NiCr wire

First, a pure copper layer was electrically deposited onto the surface of the NiCr wire by copper-plating with various electroplating times (t_e), including 3, 7, 10, 60, 80, and 100 s. A 1-V potential was applied using a DC power supply (E3664A, Agilent Technologies). Next, the electrodeposited samples were annealed for 10 min at 300°C in air to develop the pseudo-fractal Cu_2O shown in Fig. 1. Such a unique morphology can only be obtained by oxidizing the pure copper electroplate by annealing in air [14,15]. The peaks in the XRD pattern (Supporting Information Fig. S1) revealed the presence of both Cu_2O and Cu after oxidation.

2.3. Pool boiling test

Supporting Information Fig. S2 is the overall schematic of the pool boiling test. A concentric-cylindrical glass chamber was built such that fluid flow in the annulus maintained the temperature of the inner glass cylinder. A thermostat bath (JEIO TECH, CW-05G) supplied constant-temperature (150°C) propylene glycol (PG with a boiling point of 188°C) to the annulus. The entire cylindrical chamber was wrapped in aluminum foil to minimize radiant heat loss. A 1-mm-thick K-type thermocouple (Omega) with an accuracy of ±0.3°C and a data recorder (MV-1000, Yokogawa) were used to measure temperatures. A DC power supply (HPS-300G, HANIL T&M CO.) was used to heat the NiCr wire. Power was increased stepwise from 0 V at a rate of 0.2 V/s until the wire broke. Aluminum plates that are chemically stable in water were used as electrodes in the inner glass chamber. All pool boiling experiments were conducted under atmospheric conditions.

2.4. Characterization

Morphologies of the pseudo-fractal Cu_2O layers were characterized by a field-emission scanning electron microscope (FE-SEM, S-5000, Hitachi) and an optical microscope (Metaphot Inspection Microscope, Nikon). The presence of Cu and Cu_2O was confirmed by X-ray diffraction (XRD, SmartLab, Rigaku). Water contact angles of the pseudo-fractal Cu_2O layers on NiCr wires were obtained by placing a water droplet onto the wire and taking snapshots with a high-speed camera (Phantom 9.1, Vision research Inc.).

3. Results and discussion

3.1. Fractal-like Cu_2O nanotexturing

SEM images in Fig. 2 show the variable morphology of the fractal-like Cu_2O layer subject to varying electroplating times (t_e) from 3 to 100 s. For short t_e (Fig. 2a, b, and c), the layer shows "rough particle" structures that have an average diameter of 550 nm with microporous spaces between particles. Dendritic growths on the particles were observed above t_e = 10 s, forming fractal-like structures that reached tens of micrometers in height

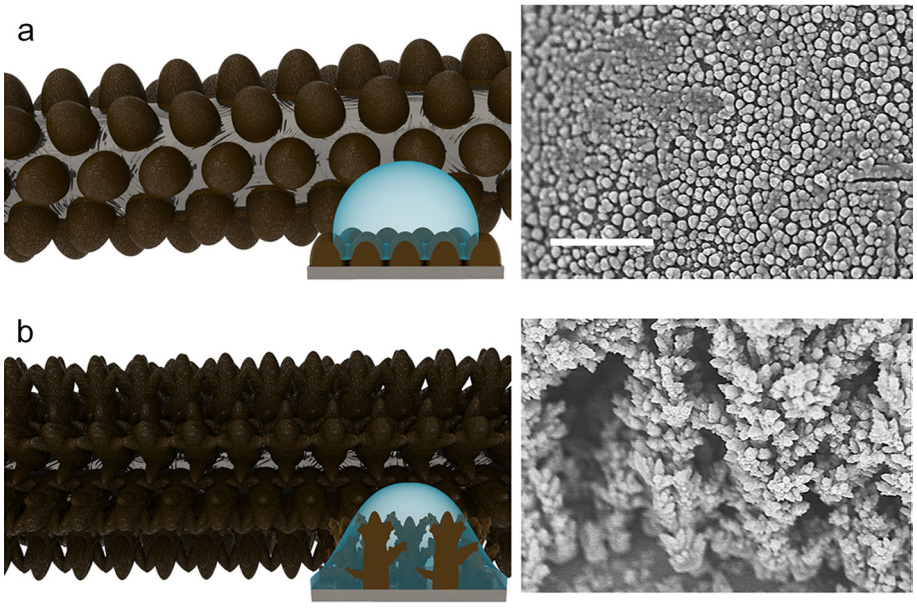

Fig. 1. Schematic and SEM images of the fractal-like Cu_2O a layers on NiCr wire as a function of the electroplating time: (a) t_e = 3 and (b) t_e = 100 s. The inset scale bar is 10 μm.

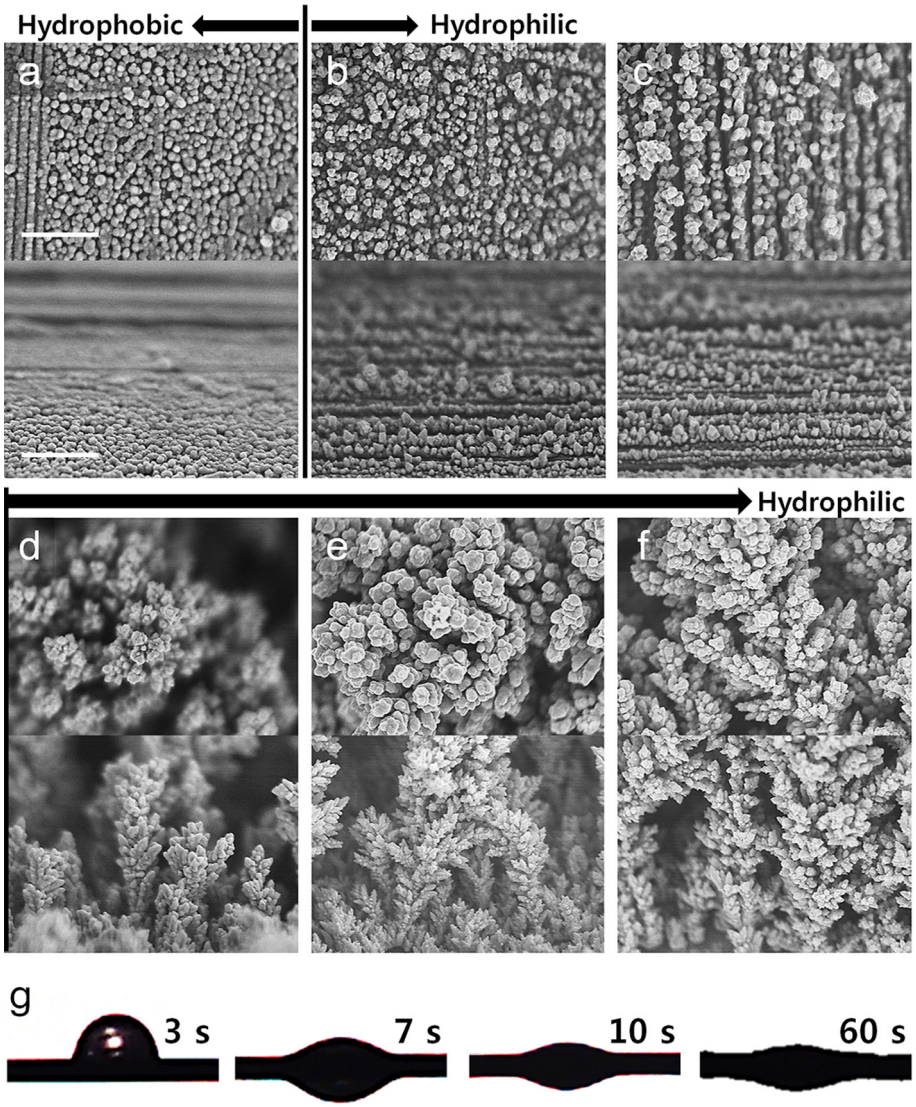

Fig. 2. Top and cross-sectional SEM images of the pseudo-fractal Cu_2O layers on a NiCr wire with electroplating times: (a) t_e = 3, (b) t_e = 7, (c) t_e = 10, (d) t_e = 60, (e) t_e = 80, and (f) t_e = 100 s. The inset scale bar is 10 μm. (g) WCA images for wires under the indicated electroplating times.

as shown in Fig. 2d, e, and f. These fractal-like structures were composed of nano- and micro-sized three-dimensional matrices and these unique structures increased the CHF by increasing the number of nucleation sites.

3.2. Effect of roughness on contact angle

Water contact angle (WCA) characterizes surface wettability, which is related to the surface energy of a substrate according to Young's equation

$$\cos\theta = \frac{\gamma_{sg} - \gamma_{sl}}{\gamma_{lg}}, \quad (1)$$

where θ is the WCA, and γ_{sg}, γ_{sl}, and γ_{lg} are the interfacial free energies per unit area of the solid-gas, solid-liquid, and liquid-gas interfaces, respectively. Note that this equation is applicable to a flat surface without roughness. For a rough surface, the dimensionless roughness, r, is expressed by the Wenzel state:

$$\cos\theta' = r\frac{\gamma_{sg} - \gamma_{sl}}{\gamma_{lg}} = r\cos\theta, \quad (2)$$

where θ' is the WCA on a rough surface; see Table 1. When the WCA of the bare wire is constant in hydrophobicity ($90° \leqslant \theta < 180°$), r increases as increasing θ' because the absolute value of $\cos\theta'$ is increased. Likewise, when the bare wire is hydrophilic ($0° \leqslant \theta < 90°$), the more θ' reduces the more r is increased because $\cos\theta'$ is higher than $\cos\theta$. For example, in the Cassie-Baxter case, increasing surface roughness induced a more hydrophobic state. On the other hand, in the Wenzel state, increasing surface roughness causes a surface to be more hydrophilic or more hydrophobic, which is the case herein when the NiCr wire was electroplated with copper as shown in Fig. 2. Cu/Cu_2O wicks were grown as increasing t_e and the roughness was increased. The tendency sucked water was

Table 1
Water contact angle (WCA), roughness factors (r), and temperature coefficient of resistance (α) on the fractal Cu_2O layers for different electroplating times. The WCA measurement uncertainty is ±4°.

t_e [s]	WCA [deg.]	r	$\alpha \cdot 10^4$ [K^{-1}]
Bare	–	–	1.60
3	72°	2.96	3.49
7	29°	8.37	4.62
10	18°	9.10	4.86
60	12°	9.36	5.01
80	~0°	~9.8	5.12
100	~0°	~9.8	5.54

increased by increasing the roughness and the water contact angle was decreased.

3.3. Data validation

The power supplied to a NiCr wire was

$$P = IV, \tag{1}$$

where I is the current and V is the voltage. Both I and V were measured quantities while the resistance, R, was estimated using the Ohm's law.

$$V = IR. \tag{2}$$

The heat flux was estimated using known V and I as:

$$q'' = \frac{VI}{A_s}, \tag{3}$$

where the surface area $A_s = \pi DL$ is a function of the wire diameter, $D = 0.296$ mm, and the wire length, $L = 30$ mm.

Electroplating the NiCr wire substantially increases the (nanostructured) surface area, which, in turn, enhances the overall convective heat transfer. However, because the exact increase in surface area is not known, the effect of the increased surface area is reflected in the effective heat transfer coefficient (h_{eff}) assuming a constant surface area. Based on Newton's convective cooling law, the effective heat transfer coefficient was estimated as:

$$h_{eff} = \frac{q''}{T_s - T_\infty}, \tag{4}$$

where T_s is the wire surface temperature and $T_\infty = 100$°C is the boiling temperature of water. Given T_∞ and q'' from Eq. (3), h_{eff} can be calculated if T_s is known. However, T_s cannot be directly measured although it can be indirectly estimated as:

$$T_s = T_{s,0} + \frac{R_s - R_{s,0}}{\alpha R_{s,0}}, \tag{5}$$

where $T_{s,0}$ is the initial wire temperature. R_s is the wire resistance varying with applied voltage ($R_s = V_s/I_s$), $R_{s,0}$ is the initial resistance measured with multimeter, and α is the resistance temperature coefficient of the wire, which is an intrinsic material property. In this case, α is a function of the Cu_2O thickness, which changes with electroplating time.

To estimate α, the electroplated wire was immersed in a water bath at room temperature $T_1 = 25$°C and then the wire resistance (R_1) was measured without Joule heating. Similarly, a second R_2 was measured at $T_2 = 100$ °C (boiling water). Using Eq. (3), α can be estimated for a given Cu_2O thickness. We repeated this procedure for all electroplated copper wires and estimated α for all cases (see Table 1). With α estimated for all Cu_2O thicknesses, the wire surface temperature (T_2 or T_s) can also be estimated using Eq. (3). Using Newton's cooling law, Eq. (4) the effective heat transfer coefficient can be experimentally estimated as shown in Fig. 3.

To verify the accuracy for the experimental data of the bare wire, the data were compared to theoretical estimates in Fig. 3a based on Rohsenow's equation, which is widely used for estimating heat flux in nucleate boiling [16]:

$$q'' = \mu_l h_v \left[\frac{g(\rho_l - \rho_g)}{\sigma}\right]^{1/2} \left(\frac{c_p \Delta T_{sat}}{C_{s,f} h_v \mathrm{Pr}_l^n}\right)^3, \tag{6}$$

where subscripts l and g represent liquid and gas, respectively, μ is fluid viscosity, h_v is the heat of vaporization, g is gravitational accel-

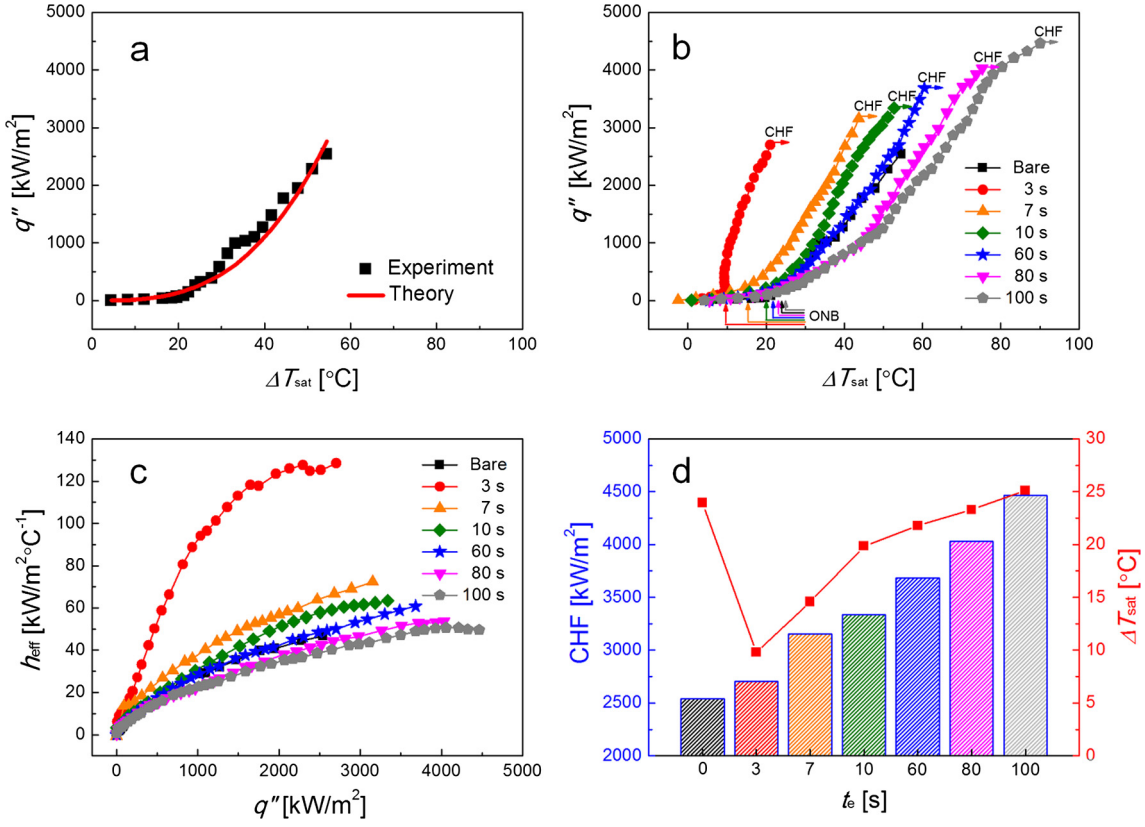

Fig. 3. (a) Comparison between the experimental and theoretical q'' for the bare NiCr wire ($t_e = 0$ s). (b) q'' versus ΔT_{sat} with t_e from 0 to 100 s. (c) h_{eff} versus ΔT_{sat} with t_e from 0 to 100 s. (d) Superheat temperature and CHF as a function of t_e. (For interpretation of the references to colour in this figure legend, the reader is referred to the web version of this article.)

eration, ρ, σ and c_p are the density, surface tension, and specific heat, respectively, and Pr is the Prantl number. $\Delta T_{sat} = T_s - T_\infty$ is the temperature difference between the wire surface and the surrounding water. Fig. 3a compares experimental and theoretical data using $n = 1$ due to water and $C_{s,f} = 0.025$ as adjustable parameters estimated by minimizing the root sum-squares differences between experimental and theoretical data [17]. This yielded an error or uncertainty range of ±3.25% for q'' [18].

3.4. Effects of nanotexturing on superheat

In general, there are four distinct regimes in pool boiling phenomena, namely free convection, nucleate boiling, transition boiling, and film boiling. In typical heat flux (q'') versus superheat (ΔT_{sat}) plots as shown in Fig. 3b, the onset of the nucleate boiling (ONB) is the points where q'' increased as indicated by the colored arrow. Early appearance of nucleate boiling at lower superheat temperatures ($\Delta T_{sat} = T_s - T_\infty$) is evidence of efficient heat transfer, which can be facilitated by nanotexturing.

In our experiment, water temperature was fixed at $T_\infty = 100$ °C while the wire surface temperature (T_s) increased according to the power input. As a result, superheat, ΔT_{sat}, increased meaning that T_s also increased. Fig. 3b, c, and d show the relation between q'', h_{eff}, and ΔT_{sat} for the various nanotextured surfaces shown in Fig. 2; i.e., $t_e = 3$, 7, 10, 60, 80, and 100 s. In Fig. 3b, q'' increased with ΔT_{sat} as the power input increased, which means that T_s increased. For $t_e = 3$ s, superheat, ΔT_{sat}, was lowest, which has the lowest T_s because $T_\infty = 100$°C. This is an interesting phenomenon as the surface morphology seen in Fig. 2a ($t_e = 3$ s) corresponds to the lowest T_s in Fig. 3b. The "rough particle" morphology shown in Fig. 2a facilitated a rapid release of bubbles because of the hydrophobic texturing. Compared to bubbles arising from the fractal-like dendrites seen in Fig. 2b–f, bubble size is larger for the morphology shown in Fig. 2a. Fig. 4a is a phenomenological illustration; bubbles are larger and are released faster on a hydrophobic surface, which cools rapidly. Rapid release of these large bubbles facilitates local cooling at the surface, which causes a decrease in T_s (and the lowest superheat). This type of rapid surface cooling finds practical application in electronics and microchip cooling as these devices malfunction when cooling is insufficient.

On the other hand, when the electroplating time increased from $t_e = 3$ s to 7, 10, 60, 80, and 100 s, the surface temperature increased for a given q''. The nucleate boiling point or superheat (where q'' begins to increase as observed in Fig. 3b) increases with t_e. This increase in superheat is presented in Fig. 3d in terms of ΔT_{sat} (red curve read on the right y axis). The reason for T_s increasing with t_e is because of the surface texturing observed in Fig. 2b – f where growing roughness increases hydrophilicity. This phenomenon is described by the Wenzel state, Eq. (2), and experimentally demonstrated in Fig. 2g, which shows the WCA on nanotextured NiCr wires for $t_e = 3$, 7, 10, and 60 s. The phenomenological description of hydrophilic pool boiling is illustrated in Fig. 4 where the surface wettability, increased due to increased surface roughness, generated more nucleation sites per unit area. However, because the surface is more hydrophilic, bubbles are attached to the surface for longer. When these bubbles stay at the surface, they hinder cooling. These bubbles are eventually released, but their increased residence times diminish cooling resulting in higher T_s. Note also that the slopes of the curves in Fig. 3b differ. These slopes, the ratio between q'' and ΔT_{sat}, are essentially the h_{eff} resulting from the nanotextured surfaces. These data are recast in Fig. 3c, where the greatest slope, or h_{eff}, is when $t_e = 3$ s. Increasing the degree of nanotexturing (or t_e), reduces h_{eff}.

3.5. Effects of nanotexturing on critical heat flux

Similarly to h_{eff}, CHF increased with t_e. CHF is the point where film boiling starts and can be estimated as the maximum q'' in each experiment (Fig. 3b). CHF increased because more nucleation sites produce more bubbles to remove heat even if the bubble release rate was slower. CHF is greatest for the longest t_e (100 s in Fig. 2f), opposite to what was observed in the superheat (ΔT_{sat} or T_s) trend. Recall that superheat is a local phenomenon while CHF is a global phenomenon. For longer t_e, increased roughness yields a higher local T_s, but more heat is removed overall due to the production of more total bubbles.

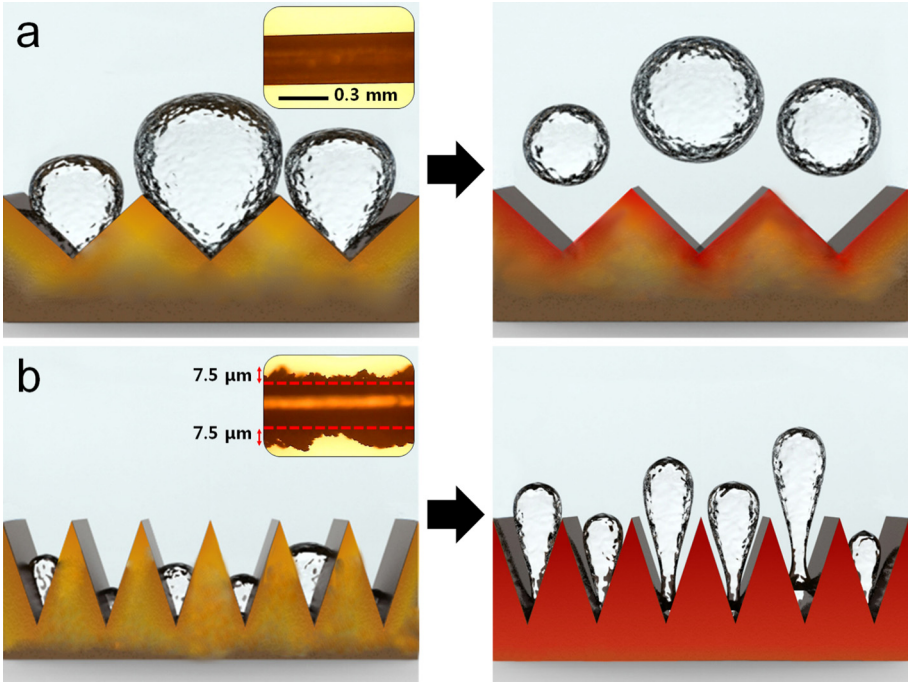

Fig. 4. Schematic of bubble formation on the surface of the fractal-like Cu_2O layers for (a) $t_e = 3$ s (hydrophobic) and (b) $t_e = 100$ s (hydrophilic).

In Fig. 3b, it is clear that CHF is lowest for the bare wire (t_e = 0 s). Upon increasing t_e, CHF increased from about 2500 to 4500 kW/m^2 as shown in Fig. 3d. Increasing roughness delayed film boiling because more heat was transferred to bubbles at the numerous nucleation sites [19,20].

Increased CHF through the fractal-like Cu_2O surfaces is illustrated in Fig. 5, which compares bubble formation for t_e = 0, 3, and 100 s. The last snapshot of these series of images is the point at which the NiCr wire failed because of excessive heating. The bubble size is clearly largest in Fig. 5a without nanotexturing. Bubble sizes decrease with increasing t_e when comparing Fig. 5a, b, and c. The most bubbles are evident in Fig. 5c, which has the highest CHF. In Fig. 5a, wire failure was captured by the CCD camera. At t = 114 s, the wire was red hot, indicating that film boiling was taking place, which prevented further cooling. A water-vapor film surrounded the wire and prevented contact between the wire and the water leading to runaway heating until wire failure. In Fig. 5b (t_e = 3 s), bubble sizes have clearly decreased because of the hydrophobic surface (Fig. 2a). For t_e = 3 s, T_s decreased, but did not significantly delay wire failure (at ~120 s) because the total volume of bubbles did not significantly increase from the bare-wire experiment. When t_e = 100 s, wire failure was delayed to 200 s, which is attributed to the increase in bubble volume (numerous small bubbles) formed on the hydrophilic surface (Fig. 2f). Overall, the CHF was greatest for the roughest surface because of the increased number of nucleation sites.

4. Conclusion

We fabricated novel fractal-like Cu_2O surfaces on a NiCr wire and identified the effects of wettability on pool boiling performance. These unique nanotextured surfaces were tuned by copper electroplating for various times to yield hydrophobic or hydrophi-

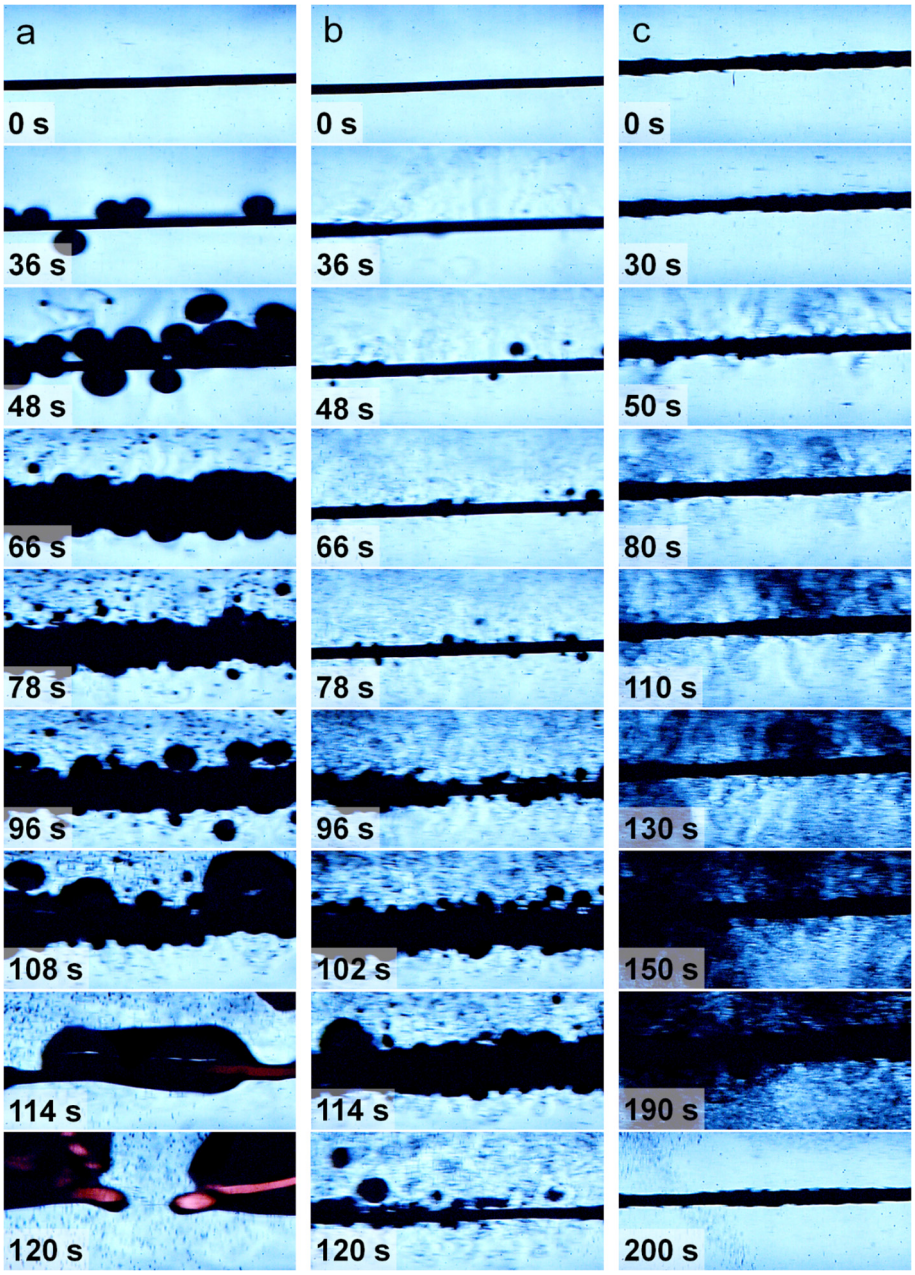

Fig. 5. Time-series snapshots of the fractal-like Cu_2O-layered wires as a function of the electroplating time: (a) t_e = 0, (b) t_e = 3, (c) t_e = 100 s.

lic surfaces. For hydrophobic surfaces, bubble release rates increased, which reduced the wire's surface temperature and corresponding superheat. Such hydrophobic texturing is desirable for electronics cooling, which demands low surface temperatures. For hydrophilic surfaces, the complicated surface structures increased the number of nucleation sites, which increased the CHF. With increased CHF, wire failure was delayed and overall cooling was improved. Both quantitative and qualitative data confirmed these trends. Finally, theoretical heat fluxes compared well with experimental data for the bare wire.

Acknowledgement

This research was supported by Global Frontier Program through the Global Frontier Hybrid Interface Materials (GFHIM) of NRF-2013M3A6B1078879 and the Commercializations Promotion Agency for R&D Outcomes (COMPA). This work was also supported by the Technological Innovation R&D Program (S2314490) funded by the Small and Medium Business Administration (SMBA, Korea). S.S. Yoon expresses his appreciation to the Vice Deanship of Scientific Research at King Saud University.

Appendix A. Supplementary data

Supplementary data associated with this article can be found, in the online version, at http://dx.doi.org/10.1016/j.ijheatmasstransfer.2016.11.029.

References

[1] A. Bar-Cohen, M. Iyengar, Design and optimization of air-cooled heat sinks for sustainable development, IEEE Trans. Compon. Packag. Technol. 25 (4) (2002) 584–591.
[2] J. Choi, M. Jeong, Compact, lightweight, and highly efficient circular heat sink design for high-end PCs, Appl. Therm. Eng. 92 (2016) 162–171.
[3] A. Faghri, Heat Pipe Science and Technology, Taylor & Francis, Washington D.C, USA, 1995.
[4] V.P. Carey, Liquid-vapor Phase-change Phenomena, second ed., CRC Press, New York, NY USA, 2008.
[5] S.-S. Hsieh, R.-Y. Lee, J.-C. Shyu, S.-W. Chen, Thermal performance of flat vapor chamber heat spreader, Energy Convers. Manage. 49 (6) (2008) 1774–1784.
[6] S. Haider, Y.K. Joshi, W. Nakayama, A natural circulation model of the closed loop, two-phase thermosyphon for electronics cooling, J. Heat Transfer 124 (5) (2002) 881–890.
[7] Y.-W. Lu, S.G. Kandlikar, Nanoscale surface modification techniques for pool boiling enhancement—a critical review and future directions, Heat Transfer Eng. 32 (10) (2011) 827–842.
[8] M. Shojaeian, A. Koşar, Pool boiling and flow boiling on micro-and nanostructured surfaces, Exp. Thermal Fluid Sci. 63 (2015) 45–73.
[9] A.S. Kousalya, K.P. Singh, T.S. Fisher, Heterogeneous wetting surfaces with graphitic petal-decorated carbon nanotubes for enhanced flow boiling, Int. J. Heat Mass Transfer 87 (2015) 380–389.
[10] S. Ujereh, T. Fisher, I. Mudawar, Effects of carbon nanotube arrays on nucleate pool boiling, Int. J. Heat Mass Transfer 50 (19) (2007) 4023–4038.
[11] V. Khanikar, I. Mudawar, T. Fisher, Effects of carbon nanotube coating on flow boiling in a micro-channel, Int. J. Heat Mass Transfer 52 (15) (2009) 3805–3817.
[12] N. Singh, V. Sathyamurthy, W. Peterson, J. Arendt, D. Banerjee, Flow boiling enhancement on a horizontal heater using carbon nanotube coatings, Int. J. Heat Fluid Flow 31 (2) (2010) 201–207.
[13] E. Forrest, E. Williamson, J. Buongiorno, L.-W. Hu, M. Rubner, R. Cohen, Augmentation of nucleate boiling heat transfer and critical heat flux using nanoparticle thin-film coatings, Int. J. Heat Mass Transfer 53 (1) (2010) 58–67.
[14] S. An, H.S. Jo, S.S. Al-Deyab, A.L. Yarin, S.S. Yoon, Nano-textured copper oxide nanofibers for efficient air cooling, J. Appl. Phys. 119 (6) (2016) 065306.
[15] S. An, H.S. Jo, D.Y. Kim, H.J. Lee, B.K. Ju, S.S. Al-Deyab, J.H. Ahn, Y. Qin, M.T. Swihart, A.L. Yarin, Self-junctioned copper nanofiber transparent flexible conducting film via electrospinning and electroplating, Adv. Mater. (2016).
[16] W.M. Rohsenow, A Method of Correlating Heat Transfer Data for Surface Boiling of Liquids, Cambridge, Mass: MIT Division of Industrial Cooperation, [1951], 1951.
[17] T.L. Bergman, F.P. Incropera, D.P. DeWitt, A.S. Lavine, Fundamentals of Heat and Mass Transfer, John Wiley & Sons, 2011.
[18] R.J. Moffat, Using uncertainty analysis in the planning of an experiment, J. Fluids Eng. 107 (2) (1985) 173–178.
[19] H. Guo, N. Lin, Y. Chen, Z. Wang, Q. Xie, T. Zheng, N. Gao, S. Li, J. Kang, D. Cai, Copper nanowires as fully transparent conductive electrodes, Sci. Rep. 3 (2013).
[20] S. An, D.-Y. Kim, J.-G. Lee, H.S. Jo, M.-W. Kim, S.S. Al-Deyab, J. Choi, S.S. Yoon, Supersonically sprayed reduced graphene oxide film to enhance critical heat flux in pool boiling, Int. J. Heat Mass Transfer 98 (2016) 124–130.